Nonlinear Dyn
https://doi.org/10.1007/s11071-018-4726-8

ORIGINAL PAPER

Breathers, solitons and rogue waves of the quintic nonlinear Schrödinger equation on various backgrounds

Stanko N. Nikolić · Omar A. Ashour · Najdan B. Aleksić · Milivoj R. Belić · Siu A. Chin

Received: 5 June 2018 / Accepted: 10 December 2018

Abstract We investigate the generation of breathers, solitons, and rogue waves of the quintic nonlinear Schrödinger equation (QNLSE) on uniform and elliptical backgrounds. The QNLSE is the general nonlinear Schrödinger equation that includes all terms up to the fifth-order dispersion. We use Darboux transformation to construct initial conditions for the dynamical generation of localized high-intensity optical waves. The condition for the breather-to-soliton conversion is provided with the analysis of soliton intensity profiles. We discover a new class of higher-order solutions in which Jacobi elliptic functions are set as background seed solutions of the QNLSE. We also introduce a method for generating a new class of rogue waves—the periodic rogue waves—based on the matching of the periodicity of higher-order breathers with the periodicity of the background dnoidal wave.

S. N. Nikolić (✉) · N. B. Aleksić
Institute of Physics Belgrade, University of Belgrade, Pregrevica 118, Belgrade 11080, Serbia
e-mail: stankon@ipb.ac.rs

S. N. Nikolić · N. B. Aleksić · O. A. Ashour · M. R. Belić
Science program, Texas A&M University at Qatar, 23874 Doha, Qatar

O. A. Ashour · S. A. Chin
Department of Physics and Astronomy, Texas A&M University, College Station, TX 77843, USA

O. A. Ashour
Department of Physics, University of California, Berkeley, CA 94720, USA

Keywords Quintic nonlinear Schrödinger equation · Darboux transformation · Rogue waves

1 Introduction

Current research on various nonlinear Schrödinger equations (NLSEs) with different dispersion and nonlinearity terms is incredibly rich and very intense, owing to their widespread use as mathematical models for physical systems in diverse fields, such as plasmas, Bose–Einstein condensates, nonlinear optics, and solid state physics [1–6]. Solitons, the solutions of NLSEs that keep their shapes during propagation and mutual interactions, as a result of balance between dispersive and nonlinear terms, are of special interest [4,6–10]. The properties revealed by the propagation and interaction of solitons play a vital role in developing many applications [11,12]. Therefore, it is important to find new soliton solutions to different physical models based on NLSEs and to study their properties.

In this paper, we study breathers, solitons, and rogue waves of the extended nonlinear Schrödinger equation, called the quintic equation

$$i\psi_x + S[\psi(x,t)] - i\alpha H[\psi(x,t)] + \gamma P[\psi(x,t)] - i\delta Q[\psi(x,t)] = 0, \tag{1.1}$$

where S, H, P, and Q are the specific operators arising in the systematic derivation of the infinite hierarchy of nonlinear Schrödinger equations [9,10]. They act on the optical slowly-varying wave envelope, denoted

Published online: 01 January 2019

by $\psi \equiv \psi(x,t)$, and systematically take into account increasing orders of dispersion and nonlinearity. As it is customary in the field of fiber optics, the transverse (temporal) variable is denoted by t and the longitudinal (spatial) variable by x.

The nonlinear Schrödinger operator S includes the basic second-order dispersion and Kerr nonlinearity:

$$S[\psi(x,t)] = \frac{1}{2}\psi_{tt} + |\psi|^2\psi. \tag{1.2}$$

The NLSE with only these terms present is the fundamental equation of nonlinear optics [13], on which the whole edifice of higher-order NLSEs and various physical models are built. The Hirota operator H encompasses the third-order dispersion and the corresponding nonlinearity [14]:

$$H[\psi(x,t)] = \psi_{ttt} + 6|\psi|^2\psi_t. \tag{1.3}$$

It is of importance in the generation of supercontinuum [8] and in pulse-deforming phenomena [15]. Operator P is called the Lakshmanan–Porsezian–Daniel (LPD) operator and it encloses the fourth-order dispersion and nonlinearity:

$$\begin{aligned} P[\psi(x,t)] = {} & \psi_{tttt} + 8|\psi|^2\psi_{tt} + 6|\psi|^4\psi + 4|\psi_t|^2\psi \\ & + 6{\psi_t}^2\psi^* + 2\psi^2\psi_{tt}^*. \end{aligned} \tag{1.4}$$

It arises in the analysis of Heisenberg spin chains [16]. The quintic operator Q includes the fifth-order terms:

$$\begin{aligned} Q[\psi(x,t)] = {} & \psi_{ttttt} + 10|\psi|^2\psi_{ttt} + 30|\psi|^4\psi_t + 10\psi\psi_t\psi_{tt}^* \\ & + 10\psi\psi_t^*\psi_{tt} + 20\psi^*\psi_t\psi_{tt} + 10\psi_t^2\psi_t^*. \end{aligned} \tag{1.5}$$

The fifth-order dispersion cannot be neglected in laser experiments producing ultrashort pulses, where the pulse duration reaches below 20 fs [17].

In Eq. (1.1), we follow the convention adopted in [16], calling the equation *quintic* and assuming that all three real parameters: α, γ and δ are in general nonzero (this is a slight change in notation as compared to [16], in which the term "quintic" is reserved for the case of $\alpha = \gamma = 0$ and $\delta \neq 0$). Also, this equation is slightly different from Eq. (1) in [18] having the same name, but including the $|\psi|^4\psi$ term with the second-order dispersion, rather than the fourth.

By setting all three parameters α, γ, and δ in Eq. (1.1) to zero, the QNLSE reduces to the basic NLSE, on which there exists a wealth of results [4,7,12,19–21]. By extending the NLSE to a more complex equation with variable coefficients, several novel optical solitary waves have been found [22]. Additional higher-order dispersion and nonlinearity terms in the NLSE are required to describe the propagation of ultrashort pulses through optical fibers [5,23–28].

Different solutions of the QNLSE, such as breathers [29,30], solitons [29,31], and rogue waves (RWs) [32], have been found and discussed in the literature. While higher-order dispersion terms are needed for a more accurate description of various propagation waves, the H, P, and Q operators (which contain more than just dispersion terms) were introduced based on the paramount concern of integrability. How best to choose the values α, γ and δ for a better, yet integral, description of any physical system remains an on-going process [9,16]. The aim of this work is to explore the impact of these higher-order nonlinear operators on breathers, solitons and rogue waves. The current work is an initial mathematical investigation rather than a final physical modeling. But, now that extensive numerical computations of these higher-order terms are available, we are in position to help experimenters in determining the optimal values of α, γ and δ for any physical system of interest.

The primary contributions of this work can be summarized as follows: (1) We presented the procedure for dynamical generation of high-intensity breathers and RWs on uniform background, based on the Darboux transformation (DT) method applied to QNLSE. (2) We provided conditions for the breather-to-soliton conversion in QNLSE and examined the transverse intensity profiles of such solitons when α, γ, and δ are nonzero. (3) We obtained new solutions of the QNLSE, when Jacobi elliptic functions (JEFs) are used as the seed waves in the DT scheme. (4) We discovered a new class of RWs, the periodic rogue waves. (5) We confirmed that the peak-height formula, introduced in [33], gives the correct peak value for all the higher-order solutions of QNLSE.

Some comments on the prior work are in order. Previously, the QNLSE has been analyzed as a specific member in the infinite NLSE hierarchy of equations [9,10]. There, new families of exact solutions have been presented that included the dnoidal/cnoidal JEFs (for an elementary introduction to JEFs, see [34]). The conversion of the breather to a soliton was analyzed in [16], but for the specific case of $\alpha = \gamma = 0$ and $\delta > 0$. Following similar lines to our combined analytical-numerical procedure for the Hirota and NLSE [35–37], here we

were able to find new solutions of QNLSE, when the dn JEF is taken as the seed wave function in the DT scheme. The algorithm is essentially the same as the one introduced in [33,35] for the Hirota equation, but the complexity of QNLSE required a more extensive and intricate numerical procedure to attain the stated goals. To this end, we extracted initial wave functions from the DT applied to the QNLSE and then propagated these functions to obtain dynamical propagating RW solutions at an arbitrary x.

In the end, we demonstrated a method for generating recurring high-intensity structures of the QNLSE on an elliptical background, which we call, paradoxically, the "periodic rogue waves". This is clearly explained in Sect. 5. Our work generalizes the procedure previously applied to the NLSE, as described in details in [38]. The new insight we bring to this work is the realization that *any* breather constructed on a periodic background will, in general, no longer be periodic. This is because the period of the breather will generally be incommensurate with the period of the background. For higher-order breathers, with more than two periods, the resulting disorder from more than two-wave mixing will destroy any periodicity, and they will therefore appear as solitary peaks on a noisy background—that is, as commonly understood RWs. However, by painstakingly matching the periods of the breathers to the background, one can resurrect the hidden periodic peaks obliterated by the background. Therefore, a new class of RWs will be produced, the *periodic* rogue waves.

This paper is organized as follows. In Sect. 2, we analyze the basic solutions of the QNLSE and show how higher-order breathers can be obtained numerically from the initial DT wave function. In Sect. 3, we provide the condition for the breather-to-soliton conversion. In Sect. 4, we present the procedure for calculating breathers and RWs on an elliptical background. In Sect. 5, we show how to build periodic RWs on a dnoidal background. In Sect. 6, we summarize our results. The general DT scheme for QNLSE is provided in "Appendix".

2 Breather solutions of the quintic equation on a uniform background

In this work, we evolve QNLSE numerically with a precisely determined initial wave function so that its intrinsic modulation instability focuses the initial wave function into breathers and RWs of different orders. The goal is to demonstrate that by adjusting the parameters of QNLSE to match realistic fiber propagation properties, the initial wave functions determined appropriately might be utilized in real experiments to produce higher-order RW structures physically. To this end, carefully chosen initial waves $\psi(x_0, t)$ at a particular value of the propagation variable $x = x_0$ are required, which can be derived by specific procedures coming from the inverse scattering theory, such as the DT. Then, the RWs are generated dynamically, by employing convenient numerical algorithms to evolve the wave function ψ over the entire (x, t) grid.

Exact first-order solutions of the infinite NLSE hierarchy are calculated in [9,10]. Here, we are interested in the more realistic case of QNLSE (1.1) and higher-order solutions. Thus, all the coefficients in the infinite hierarchy multiplying the sixth and higher-order dispersions will be set to zero, while the initial waves will be carefully chosen, so as to generate solutions of different orders. The solution procedure is as follows.

According to the inverse scattering theory of NLSE, the first-order breather solution $\psi_1(x, t)$, characterized by the complex eigenvalue

$$\lambda = r + i\nu, \tag{2.1}$$

is obtained from the DT scheme having the $\psi_0 = \mathrm{e}^{i(1+6\gamma)x}$ plane-wave seed. It is of the form:

$$\psi_1(x,t) = \left(1 + 2\nu\frac{G_1 + iH_1}{D_1}\right)\mathrm{e}^{i(1+6\gamma)x}. \tag{2.2}$$

Here:

$$\begin{aligned} G_1 &= \cos(\kappa_r t + d_r x)\cosh(2\chi_i) \\ &\quad - \cosh(\kappa_i t + d_i x)\sin(2\chi_r), \\ H_1 &= \sinh(\kappa_i t + d_i x)\cos(2\chi_r) \\ &\quad + \sin(\kappa_r t + d_r x)\sinh(2\chi_i), \\ D_1 &= \cosh(\kappa_i t + d_i x)\cosh(2\chi_i) \\ &\quad - \cos(\kappa_r t + d_r x)\sin(2\chi_r), \end{aligned} \tag{2.3}$$

where the wavenumbers, frequencies and other parameters are:

$$\begin{aligned} \kappa &= 2\sqrt{1+\lambda^2} = \kappa_r + i\kappa_i \\ \chi &= \frac{1}{2}\arccos\left(\frac{\kappa}{2}\right) = \chi_r + i\chi_i \\ \bar{d} &= 2(\alpha+3\delta) + (1+4\gamma)\lambda - 4(\alpha+2\delta)\lambda^2 \\ &\quad - 8\gamma\lambda^3 + 16\delta\lambda^4 \left(\bar{d} = \bar{d}_r + i\bar{d}_i\right) \\ d &= \kappa\bar{d} = d_r + id_i. \end{aligned} \tag{2.4}$$

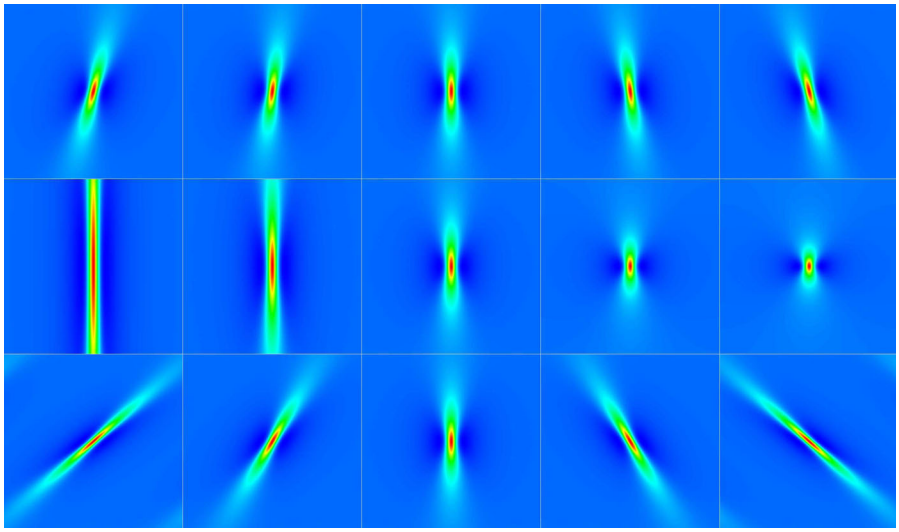

Fig. 1 First-order breather intensity distribution in the (x, t) plane for different values of parameters α, γ and δ. The eigenvalue is $\lambda \approx 0.97i$. In each row, one parameter is varied and the other two are set to zero. Top row: $\gamma = 0$, $\delta = 0$, $\alpha = -0.10, -0.05, 0, +0.05, +0.10$, from left to right. Middle row: $\alpha = 0, \delta = 0, \gamma = -0.10, -0.05, 0, +0.05, +0.10$, from left to right. Bottom row: $\alpha = 0$, $\gamma = 0$, $\delta = -0.10, -0.05, 0, +0.05, +0.10$, from left to right. In each panel, the transverse axis (horizontal) spans from $t = -6.3$ to 6.3 and the propagation axis (vertical) from $x = -2.5$ to 2.5

One can see that ψ_1 is periodic in the transverse direction (with the imaginary part of the eigenvalue $0 < \nu < 1$), i.e., it represents a breather. The frequency ω and the period L are solely determined by the imaginary part of the eigenvalue:

$$\omega = 2\sqrt{1-\nu^2}, \quad L = \frac{\pi}{\sqrt{1-\nu^2}}. \tag{2.5}$$

In Fig. 1, we show the first-order breathers with purely imaginary eigenvalues, to depict the influence of the QNLSE parameters α, γ and δ on the intensity distribution of ψ_1 in the (x, t) plane. In the top row, we varied parameter α from -0.1 to $+0.1$, keeping $\gamma = 0$ and $\delta = 0$. Analogously, in the middle (bottom) row, we changed only γ (δ) value. One can see that the larger absolute value of α introduces the bigger skew of the breather, while the sign of α determines to which side the breather is tilted. The parameter γ does not introduce the skew, but extends ($\gamma < 0$) or compresses ($\gamma > 0$) the breather along the evolution x-axis. As for δ, it also skews the breather (but stronger than α) and narrows its intensity profile. These observations also hold for the breathers on nonuniform backgrounds and for higher-order breathers (i.e., RWs) that will be covered in the next sections. These, as it will be seen, can be calculated via a recursive DT scheme using the same seed for a given set of eigenvalues.

In order to create the Nth-order QNLSE breather dynamically, we have to preserve the fundamental periodicity of ψ_1 and thus choose periodic boundary conditions in numerics. The details of the procedure are given in [33,35]. Now, there are N eigenvalues, and we assume that initially each of these eigenvalues is purely imaginary $\lambda_j = i\nu_j$. We choose the eigenvalues such that the higher-order frequencies are equal to the integer multiples of the first-order frequency: $\omega_j = j\omega$ ($\nu_1 \equiv \nu$, $\omega_1 \equiv \omega$). It follows:

$$\lambda_j = i\nu_j = i\sqrt{j^2\nu^2 - (j^2-1)} \quad \text{for} \quad 2 \le j \le N. \tag{2.6}$$

The procedure is to take the initial ν, calculate other eigenvalues using the last equation and apply the DT, to calculate the appropriate initial wave condition across the transverse t-axis. That wave is then evolved numerically, starting from some value of x before the desired peak of the rogue wave and ending well past the peak. For numerical integration, we use a finite difference method, to calculate the derivatives up to fifth-order and the fourth-order explicit Runge–Kutta method for the evolution of the wave function. Due to the complexity and high nonlinearity of the quintic equation,

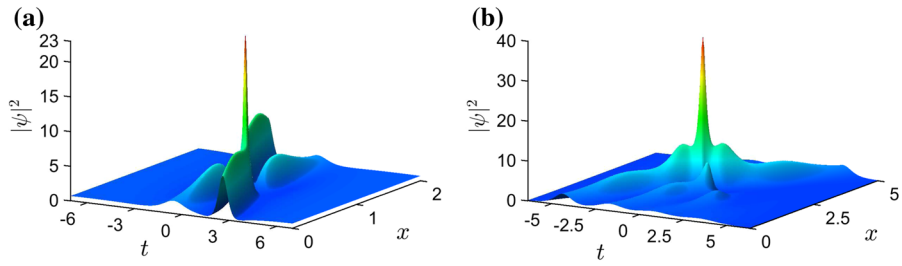

Fig. 2 Dynamically generated higher-order breathers of QNLSE on a uniform background. Initial wave functions are extracted from the DT solutions and then numerically evolved along coordinate x. The values of ν_1 are set at the beginning of the procedure, while other imaginary parts are calculated using Eq. (2.6). **a** The second-order breather: $\nu_1 = \sqrt{0.95}$, $\alpha = 0.0625$, $\gamma = 0.053$, $\delta = 0.043$. **b** The fourth-order breather: $\nu_1 = \sqrt{0.9384}$, $\alpha = -0.1625$, $\gamma = 0.017$, $\delta = 0.006$

derivatives are calculated with $O(h^{12})$ accuracy, where h is the step size along the t-axis.

In Fig. 2, we demonstrate the second- and fourth-order breathers obtained dynamically. In Fig. 2a, we choose $\nu_1 = \sqrt{0.95}$ for the first constituent breather and calculate ν_2 using Eq. (2.6). The parameters are: $\alpha = 0.0625$, $\gamma = 0.053$, and $\delta = 0.043$. In Fig. 2b, it is $\nu_1 = \sqrt{0.9384}$, $\alpha = -0.1625$, $\gamma = 0.017$, and $\delta = 0.006$. As explained before, the tilt and the stretching of breathers are caused by the QNLSE parameters. We also confirm that the peak intensities ($|\psi|^2_{\max} = 22.453$ in Fig. 2a and $|\psi|^2_{\max} = 39.029$ in Fig. 2b) are determined solely by the imaginary parts of eigenvalues, independent of α, γ, δ, in agreement with the peak-height formula derived in our previous work [33,35]. In fact, the same conclusion holds for the infinite hierarchy of NLSEs.

3 Breather-to-soliton conversion in the quintic equation

Usually, solitons cannot be obtained from breathers. However, in QNLSE, for the specific values of α, γ, and δ, the solitons can be directly obtained from the breather solutions. The breather-to-soliton conversion happens when the extrema of trigonometric and hyperbolic functions in Eq. (2.3) are located along the same straight lines in the (x,t) plane [16]. From Eq. (2.3), one can write:

$$\frac{d_r}{\kappa_r} = \frac{d_i}{\kappa_i}. \tag{3.1}$$

From this equation and Eq. (2.4), it follows:

$$\bar{d}_i = 0. \tag{3.2}$$

Assuming a general complex eigenvalue $\lambda = r + i\nu$, we use Eqs. (2.3) and (3.2) to derive a relation between α, γ, δ, and ν for which the breather-to-soliton conversion emerges:

$$8r\left(8r^2\delta - 3r\gamma - \alpha - 2\delta\right) + 8\nu^2(\gamma - 8r\delta) + 4\gamma + 1 = 0. \tag{3.3}$$

The soliton obtained in this manner is characterized by oscillatory tails at both sides of the central maximum. If we analyze the transverse soliton profile at $x = 0$, we see from Eq. (2.3) that the modulus of the wave function ψ is determined by the ratio of $\cos(\kappa_r t)$ to $\cosh(\kappa_i t)$. It follows that the number of side fringes depends on the quantity κ_r/κ_i. Similar "multi-peak" and W-shaped solitons were reported for the LPD equation, that is, Eq. (1.1) with $\alpha = \delta = 0$ [39,40].

In Fig. 3, we show two breather-to-soliton conversions under the condition of Eq. (3.3). One chooses the real and imaginary parts of eigenvalue λ and of the two quintic parameters. The remaining parameter is then computed by Eq. (3.3). The soliton in Fig. 3a is formed for $\lambda = 0.75 + 0.9i$, $\alpha = 0.75$, $\gamma = -0.12$, $\delta = -0.13139$. For the soliton in Fig. 3b, we have $\lambda = 0.057 + 0.85i$, $\alpha = \frac{1}{12}$, $\gamma \approx -0.08397$, $\delta = \frac{1}{24}$. In the first case, one sees one fringe at both sides of the soliton maximum, due to the low $k_r/k_i \approx 1.7$ ratio. In the second case, several fringes are seen, since $\kappa_r/\kappa_i \approx 6$.

4 Solutions of the quintic equation on an elliptical background

Rogue waves in nature never appear on a flat background. There is always a wavy background, on which

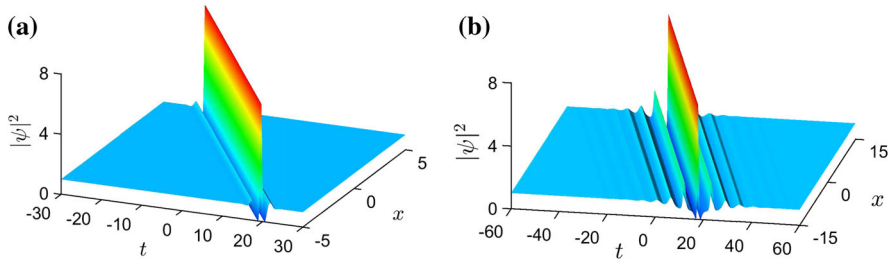

Fig. 3 Conversion of the first-order breather of QNLSE to a soliton: **a** $\lambda = 0.75 + 0.9i$, $\alpha = 0.75$, $\gamma = -0.12$, $\delta = -0.13139$ and $\kappa_r/\kappa_i \approx 1.7$, **b** $\lambda = 0.057 + 0.85i$, $\alpha = \frac{1}{12}$, $\gamma \approx -0.08397$, $\delta = \frac{1}{24}$ and $\kappa_r/\kappa_i \approx 6$

under certain circumstances suddenly giant waves appear. Therefore, of particular interest are localized solutions that grow on nonuniform backgrounds [35]. It is shown in [37] that the general form of NLSE solution on an elliptical background can include only two JEFs, cn or dn. We generalize this finding to the QNLSE.

Exact solutions of the QNLSE that include JEFs are presented in [9,10]:

$$\psi_{\rm dn}(x,t) = c\mathrm{e}^{i\phi x}\,\mathrm{dn}\,(ct + vx, m)\,, \tag{4.1}$$

$$\psi_{\rm cn}(x,t) = \frac{c}{\sqrt{2}}\sqrt{s+1}\mathrm{e}^{i\phi x} \cdot \mathrm{cn}\left(\sqrt{s}ct + \sqrt{s}vx, m = \frac{1}{2} + \frac{1}{2s}\right). \tag{4.2}$$

Here we produce analogous solutions dynamically. With $m = g^2$ we denote the elliptic modulus squared, c is an arbitrary constant, while ϕ and v are quantities determined by α, γ, δ, m, and c, as specified below. We can use any of these functions as a seed in the DT scheme to calculate the Nth-order breathers on elliptical backgrounds. The matrices U and V, necessary for the DT scheme of the quintic NLSE, are given in "Appendix".

Note that all results obtained for the Hirota equation and presented in [35], can be obtained by the method of this section, when $\gamma = \delta = 0$ is chosen. However, here we aim at obtaining more general solutions of the QNLSE.

4.1 Applying the DT scheme to $\psi_0 = \psi_{\rm dn}$

We now apply the DT procedure, as described in "Appendix". We first examine the case when the seed function ψ_0 is given by Eq. (4.1), with $\phi = \frac{1}{2}(2-m)c^2 + \gamma c^4(6 - 6m + m^2)$ and $v = (2-m)\alpha c^3 + \delta c^5(6 - 6m + m^2)$ [10]. To solve a system of four coupled linear differential equations for Lax pairs r_t, s_t, r_x and s_x (subscripts indicate partial derivatives), we use the traveling wave variable u

$$u = ct + vx, \tag{4.3}$$

and replace the t-derivatives with the u-derivatives. Having in mind the form of equations, we try the solutions of the form:

$$r(x,u) = g(x,u)\mathrm{e}^{-i\phi x/2}, \quad s(x,u) = h(x,u)\mathrm{e}^{+i\phi x/2}. \tag{4.4}$$

We skip the derivation details, which can be found in [35]. First, one finds the u-derivatives of g and h:

$$g_u = i\frac{\lambda}{c}g + i \cdot \mathrm{dn}(u)h, \tag{4.5}$$

$$h_u = i \cdot \mathrm{dn}(u)g - i\frac{\lambda}{c}h. \tag{4.6}$$

Next, one provides the constants A and B for the quintic case (cf. "Appendix"):

$$A = \left(4\lambda^2 - mc^2\right)\left(\frac{1}{4} - \alpha\lambda\right) + (\gamma - 2\delta\lambda)\left[4\lambda^2\left(c^2 - 2\lambda^2\right) - \frac{1}{2}mc^4\,(2-m)\right], \tag{4.7}$$

$$B = c\lambda\left[(1 - 4\alpha\lambda) + 2\,(\gamma - 2\delta\lambda)\left[(2-m)c^2 - 4\lambda^2\right]\right]. \tag{4.8}$$

The solution for the Lax pair generating functions, with the eigenvalues λ_j and x-shifts x_{0j} $(1 \le j \le N)$ is:

$$r_{1j}(x, u=0) = 2i\mathrm{e}^{-i\phi(x-x_{0j})/2} \cdot \sin[+\chi_j + \kappa_j\lambda_j(x - x_{0j}) - \pi/4], \tag{4.9}$$

$$s_{1j}(x, u=0) = 2\mathrm{e}^{+i\phi(x-x_{0j})/2} \cdot \cos[-\chi_j + \kappa_j\lambda_j(x - x_{0j}) - \pi/4], \tag{4.10}$$

where:

$$\kappa_j = \frac{\sqrt{A_j^2 + B_j^2}}{\lambda_j}, \tag{4.11}$$

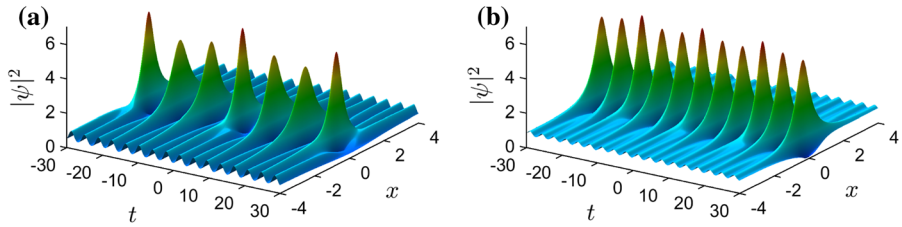

Fig. 4 First-order breathers on the dn background. The parameters are: $c = 1, \lambda = 0.75i, \alpha = 0.13, \gamma = 0.1, \delta = -0.07$: **a** $m = 0.75^2$ and **b** $m = 0.5^2$. As m decreases, the breather appears more periodic

$$\chi_j = \frac{1}{2} \arccos \frac{\kappa_j \lambda_j}{B_j}. \tag{4.12}$$

Constants A and B (and thus κ and χ) are labeled with the j index and are calculated for each $\lambda \equiv \lambda_j$.

Now, we need to calculate $r_{1,j}$ and $s_{1,j}$ for any u. The evolution equations are given by expressions (4.5) and (4.6). We can solve them numerically, using the fourth-order Runge–Kutta method. We write $u = ct + v(x - x_0) = 0$ and get $t = -\frac{v}{c}(x - x_0)$. Starting from this value of t and by numerically evolving $\mathrm{d}u = c\mathrm{d}t$ (at a given x in the grid), one can calculate $r_{1,j}(x, u)$ and $s_{1,j}(x, u)$. Next, we shift these values to the entire (x, t) plane, to get $r(x, t)$ and $s(x, t)$. Finally, one employs Eqs. (A 1) and (A 2) to calculate the Nth-order solution $\psi_N(x, t)$.

In Fig. 4, we show the first-order breather ($\lambda = 0.75i$) on an oscillatory dn background, for different values of m. The parameters are: $c = 1$, $\alpha = 0.13$, $\gamma = 0.1$, and $\delta = -0.07$. For (a) $m = 0.75^2$ and for (b) $m = 0.5^2$. Whereas breathers on a constant background are strictly periodic, except at $\lambda = i$, when one obtains the Peregrine soliton, the peaks here are aperiodic. This is easily understandable because we now have two periods, that of the breather, and that of the background. When the two periods are incommensurate, no overall periodicity is possible. We thus see the quasi-periodic oscillation of the peaks with increasing value of m. The spacing between the peaks can also be understood as the beat phenomenon associated with having two periods. As shown, there are only 7 peaks for $m = 0.75^2$ but 11 for $m = 0.5^2$. In the limit of $m \to 0$, one recovers the constant background case. For this case of first-order breathers, having two periods only changes periodicity to quasi-periodicity. As we will see in Sect. 5, for higher-order breathers involving more than two periods, the changes will be more dramatic.

4.2 Applying the DT scheme to $\psi_0 = \psi_{\mathrm{cn}}$

The seed function ψ_0 is now given by Eq. (4.2), where $\phi = \frac{1}{2}c^2 + \frac{1}{2}\gamma c^4(3 - s^2)$ and $v = \alpha c^3 + \frac{1}{2}\delta c^5(3 - s^2)$. We again consider the traveling wave variable u and continue working in the xu-grid:

$$u = \sqrt{s}\,(ct + vx)\,. \tag{4.13}$$

Following the procedure from the previous subsection, we get for the values of A and B:

$$A = \left[\lambda^2 - \frac{c^2}{4\,(2m-1)}\right] \cdot [1 - 4\alpha\lambda + 2(\gamma - 2\delta\lambda)(c^2 - 4\lambda^2)], \tag{4.14}$$

$$B = c\lambda\sqrt{\frac{m}{2m-1}}[1 - 4\alpha\lambda + 2(\gamma - 2\delta\lambda)(c^2 - 4\lambda^2)]. \tag{4.15}$$

The Lax pair generating functions $r_{1j}(x, u = 0)$ and $s_{1j}(x, u = 0)$, as well as κ_j and χ_j, all have the same *general* form as for the dn seedings—Eqs. (4.9) to (4.12). However, κ_j and χ_j differ in the two cases, due to different A and B for the dn/cn seeds, and therefore r, s and the final solution $\psi_N(x, t)$ will differ too.

5 Periodic rogue waves

In this section, we show that the appearance of RW solutions in the QNLSE is determined by the interaction of the periods of a higher-order breather with that of the dn background.

In Fig. 5a, we show a second-order breather generated with $\nu_1 = 0.92$, $\nu_2 = 0.81$, and quintic parameters $c = 1$, $m = 0.1049$, $\alpha = 0.05$, $\gamma = -0.003$ and $\delta = 0.5$. Similar to the first-order breather case of Fig. 4, the peaks are not periodic. For the second and higher-order breathers, the mixing of three or more modes generally leads to chaos, and the periodicity

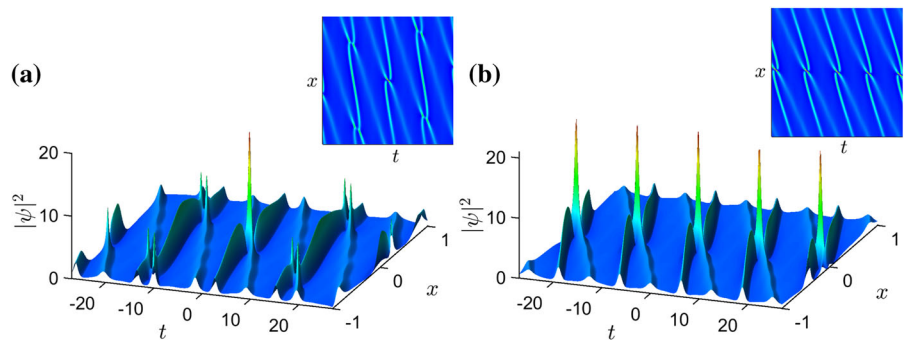

Fig. 5 Second-order breather on a dn background. Parameters: $c = 1$, $m = 0.1049$, $\alpha = 0.05$, $\gamma = -0.003$, $\delta = 0.5$. **a** Unmatched case, when only the central RW peak is generated: $\nu_1 = 0.92$, $\nu_2 = 0.81$, $q = 3.17$. **b** Periodic rogue wave. Constituent breathers are matched mutually and to the dn background wave: $\nu_1 = 0.94$, $\nu_2 = 0.8345$, $q = 4$. Insets in both figures show the 2D-intensity distributions, depicting high-intensity peaks imposed on the elliptic background. Note the appearance of the slanted secondary RW peaks in (**a**), suggesting the possibility of building a Talbot carpet out of RWs

is destroyed. Therefore, one sees in Fig. 5a, only a solitary peak on a noisy background. *Thus, higher-order breathers on a periodic background are generally rogue waves*. On a periodic background, there is therefore a radical distinction between first-order breathers and all higher-order breathers.

What happens now if one insists that the higher-order breather's period matches that of the background?

The period of the dnoidal part of the DT seed function [Eq. (4.1) with $c = 1$] is given by:

$$T_{\rm dn} = 2K(m) = 2\int_0^{\pi/2} \frac{{\rm d}\theta}{\sqrt{1 - m\sin^2\theta}}, \tag{5.1}$$

where $K(m)$ is the complete elliptic integral of the first kind. On the other hand, from the exact solution of the Lax pair along the $u = 0$ line (Sect. 4), one can write the characteristic breather period as:

$$T_{\rm B} = \frac{\pi}{\kappa_r}. \tag{5.2}$$

Here $\kappa = \kappa(\alpha, \gamma, \delta, \nu, m) = \kappa_r + i\kappa_i$ is given by Eq. (4.11). In order for the breather's period to be commensurate with that of the *dn* function, one must match

$$\frac{\pi}{\kappa_r} = 2qK(m) \;\Rightarrow\; \kappa_r = \frac{\pi}{2qK(m)}, \tag{5.3}$$

for some positive integer q. This matching requires two steps. (1) After some values of α, γ, δ and ν_1 are chosen, one writes the general expression for κ_1 and the breather period $T_{\rm B1}$ using Eqs. (4.7), (4.8), (4.11) and (5.2). Then, one numerically solves Eq. (5.3) to find m for given ν and q (note that this procedure can be inverted, i.e. one can calculate ν_1 for the given m). (2) One matches the periods of all constituent breathers by numerically solving the set of $N - 1$ equations:

$$T_{{\rm B}j} = T_{\rm B1}/j, \quad \text{where} \quad j = 2, \ldots, N. \tag{5.4}$$

In this way, one calculates $\nu_2, \ldots, \nu_N$. Having the complete set of breather frequencies, the wave function $\psi_N(x, t)$ can be calculated using DT (see Sect. 4.1).

For the same set of quintic parameters as used in Fig. 5a, we now take $\nu_1 = 0.94$, giving $q = 4$, meaning that the period of the first constituent breather is four times larger than the period of the dn seed function (4.1). Next, we determine ν_2 of the second constituent breather from $T_{\rm B2} = T_{\rm B1}/2$ to be $\nu_2 = 0.8345$. Now both breather's periods are commensurate to the background and to each other. The resulting second-order breather is shown Fig. 5b. One now sees a periodic series of peaks of nearly equal height as that of Fig. 5a. Clearly, if Fig. 5a is a rogue wave, then Fig. 5b is a *periodic rogue wave*.

We repeat the procedure for a third-order breather, keeping the same values of c, m, α, γ, δ and ν_1 as in the previous figure. The results are depicted in Fig. 6. Again, if we just take $\nu_2 = 0.81$ and $\nu_3 = 0.61$, with periods unmatched to the background, one obtains a RW shown in Fig. 6a. However, if one takes $\nu_2 = 0.8345$ and $\nu_3 = 0.625$, matching the background period, then one obtains the periodic RW of Fig. 6b. Note that the peaks are lying along a skewed line in the (x, t) plane, not along the t-axis.

If one changes the elliptic modulus squared m sufficiently, while keeping the breather's eigenvalues intact, the RW periodicities would also be disturbed (not

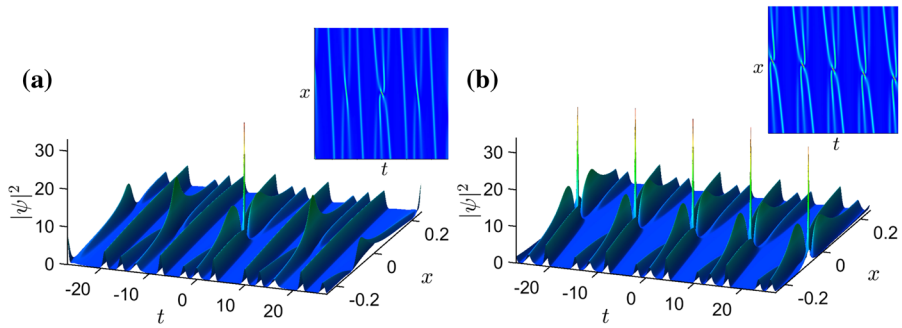

Fig. 6 Third-order breather on a dn background. Parameters: $c = 1$, $m = 0.1049$, $\alpha = 0.05$, $\gamma = -0.003$, $\delta = 0.5$. **a** An unmatched case when only the central RW peak is generated: $\nu_1 = 0.92$, $\nu_2 = 0.81$, $\nu_3 = 0.61$, $q = 3.17$. **b** Periodic RW. The constituent breathers are matched mutually and to the dn background wave: $\nu_1 = 0.94$, $\nu_2 = 0.8345$, $\nu_3 = 0.625$, $q = 4$. Insets in both figures show the 2D-intensity distributions, depicting high-intensity peaks imposed on the elliptical background

shown). We stress the fact that the third-order periodic RWs are harder to obtain and are more vulnerable to the mismatch of the frequencies, when compared to the second-order breathers. Also, the possibility of building Talbot carpets with the third-order periodic RWs appears more remote. Namely, the modulation instability of the third-order solutions is greater and the probability of three different modes constructively interfering in the (x, t) plane is significantly lower.

We also confirm the validity of the peak-height formula for the dn background (Figs. 4, 5, 6), since it exactly reproduces the maximum intensity of the central peak at $(0, 0)$ (not shown). This further points to the universal validity of the peak-height formula for all members of the infinite hierarchy of NLSEs.

6 Conclusion

In this paper, we have presented a procedure for the dynamical generation of breathers and RWs of the QNLSE on uniform and elliptical backgrounds. We have derived the condition for the breather-to-soliton conversion of QNLSE for nonzero α, γ, and δ parameters, and provided an analysis of intensity profiles of a converted soliton.

We have obtained various intense solitary or periodic peaks for the highly nonlinear and computationally demanding QNLSE. In many aspects, our procedure can be termed as an exact procedure for obtaining numerical RWs of the QNLSE. In this way, one can construct and analyze unstable higher-order solutions due to the modulation instability. They could be of importance for the production of exotic solutions in physical systems modeled by the QNLSE.

But most importantly, we have pointed out a radical distinction between the first-order breathers and all higher-order breathers on a periodic background. The first-order breathers can at most be quasi-periodic, whereas all higher-order breathers are generally RWs. By matching the period of the breather to that of the background, which requires exceedingly fine tuning, one can generate a new and even more rare kind of RWs, which, paradoxically, are *periodic*.

Acknowledgements This research is supported by the Qatar National Research Fund (Project NPRP 8-028-1-001). S.N.N. acknowledges support from Grants III 45016 and OI 171038 of the Serbian Ministry of Education, Science and Technological Development. N.B.A. acknowledges support from Grant OI 171006 of the Serbian Ministry of Education, Science and Technological Development. O.A.A. is supported by the Berkeley Graduate Fellowship and the Anselmo J. Macchi Graduate Fellowship. M.R.B. acknowledges support by the Al-Sraiya Holding Group.

Compliance with ethical standards

Conflict of interest The authors declare that they have no conflict of interest.

Appendix A: The general Darboux transformation scheme

The quintic solution of order N is a nonlinear superposition of N independent simple solutions, where each is determined by the complex eigenvalue λ_j $(1 \leq j \leq$

N). The corresponding wave function is:

$$\psi_n = \psi_{n-1} + \frac{2\left(\lambda_n^* - \lambda_n\right) s_{n,1} r_{n,1}^*}{\left|r_{n,1}\right|^2 + \left|s_{n,1}\right|^2}. \tag{A 1}$$

The Lax pair functions $r_{n,1}$ and $s_{n,1}$ are given by recursive relations involving $r_{n,p}(x,t)$ and $s_{n,p}(x,t)$:

$$\begin{aligned} r_{n,p} = &\left[\left(\lambda_{n-1}^* - \lambda_{n-1}\right) s_{n-1,1}^* r_{n-1,1} s_{n-1,p+1}\right. \\ &+ \left(\lambda_{p+n-1} - \lambda_{n-1}\right) \left|r_{n-1,1}\right|^2 r_{n-1,p+1} \\ &\left.+ \left(\lambda_{p+n-1} - \lambda_{n-1}^*\right) \left|s_{n-1,1}\right|^2 r_{n-1,p+1}\right] \\ &\Big/ \left(\left|r_{n-1,1}\right|^2 + \left|s_{n-1,1}\right|^2\right), \\ s_{n,p} = &\left[\left(\lambda_{n-1}^* - \lambda_{n-1}\right) s_{n-1,1} r_{n-1,1}^* r_{n-1,p+1}\right. \\ &+ \left(\lambda_{p+n-1} - \lambda_{n-1}\right) \left|s_{n-1,1}\right|^2 s_{n-1,p+1} \\ &\left.+ \left(\lambda_{p+n-1} - \lambda_{n-1}^*\right) \left|r_{n-1,1}\right|^2 s_{n-1,p+1}\right] \\ &\Big/ \left(\left|r_{n-1,1}\right|^2 + \left|s_{n-1,1}\right|^2\right). \end{aligned} \tag{A 2}$$

Thus, all pairs $r_{n,p}$ and $s_{n,p}$ can be determined starting from $r_{1,j}$ and $s_{1,j}$. The functions $r_{1,j}(x,t)$ and $s_{1,j}(x,t)$, forming the Lax pair $R = \begin{pmatrix} r \\ s \end{pmatrix} \equiv \begin{pmatrix} r_{1,j} \\ s_{1,j} \end{pmatrix}$, are determined by the eigenvalue $\lambda \equiv \lambda_j$ and an embedded arbitrary center of the solution (x_{0j}, t_{0j}). The Lax pair satisfies a system of linear differential equations:

$$\frac{\partial R}{\partial t} = U \cdot R, \quad \frac{\partial R}{\partial x} = V \cdot R. \tag{A 3}$$

For the quintic NLSE, matrices U and V are defined as ($\psi \equiv \psi_0$) [31]:

$$\begin{aligned} U &= i \begin{bmatrix} \lambda & \psi(x,t)^* \\ \psi(x,t) & -\lambda \end{bmatrix}, \\ V &= \sum_{k=0}^{5} \lambda^k \cdot i \begin{bmatrix} A_k & B_k^* \\ B_k & -A_k \end{bmatrix}. \end{aligned} \tag{A 4}$$

The coefficients A_k and B_k are given by:

$$\begin{aligned} A_0 = &-\frac{1}{2}|\psi|^2 - 3\gamma|\psi|^4 - i\alpha\left(\psi_t^*\psi - \psi_t\psi^*\right) \\ &-\gamma\left(\psi_{tt}^*\psi - |\psi_t|^2 + \psi_{tt}\psi^*\right) \\ &-i\delta\left(\psi_{ttt}^*\psi - \psi_{tt}^*\psi_t + \psi_{tt}\psi_t^* - \psi_{ttt}\psi^*\right) \\ &-6i\delta\left(\psi_t^*\psi - \psi_t\psi^*\right)|\psi|^2, \\ B_0 = &\, 2\alpha|\psi|^2\psi + 6\delta|\psi|^4\psi + i\frac{1}{2}\psi_t + 6i\gamma|\psi|^2\psi_t \\ &+\alpha\psi_{tt} + 2\delta\psi_{tt}^*\psi^2 + 4\delta|\psi_t|^2\psi + 6\delta(\psi_t)^2\psi^* \\ &+8\delta\psi_{tt}|\psi|^2 + i\gamma\psi_{ttt} + \delta\psi_{tttt}, \\ A_1 = &\, 2\alpha|\psi|^2 + 6\delta|\psi|^4 - 2i\gamma\left(\psi_t^*\psi - \psi_t\psi^*\right) \\ &+2\delta\left(\psi_{tt}^*\psi - |\psi_t|^2 + \psi_{tt}\psi^*\right), \\ B_1 = &\, \psi + 4\gamma|\psi|^2\psi - 2i\alpha\psi_t - 12i\delta|\psi|^2\psi_t \\ &+2\gamma\psi_{tt} - 2i\delta\psi_{ttt}, \\ A_2 = &\, 1 + 4\gamma|\psi|^2 + 4i\delta\left(\psi_t^*\psi - \psi_t\psi^*\right), \\ B_2 = &-4\alpha\psi - 8\delta|\psi|^2\psi - 4i\gamma\psi_t - 4\delta\psi_{tt}, \\ A_3 = &-4\alpha - 8\delta|\psi|^2, \\ B_3 = &-8\gamma\psi + 8i\delta\psi_t, \\ A_4 = &-8\gamma, \\ B_4 = &\, 16\delta\psi, \\ A_5 = &\, 16\delta, \\ B_5 = &\, 0. \end{aligned} \tag{A 5, A 6}$$

The solutions of Lax pair equations are further pursued in the text.

References

1. Bao, W.: The nonlinear Schrödinger equation and applications in Bose–Einstein condensation and plasma physics. In: Lecture Note Series, IMS, NUS, vol. 9 (2007)
2. Shukla, P.K., Eliasson, B.: Nonlinear aspects of quantum plasma physics. Phys. Usp. **53**, 51 (2010)
3. Busch, T., Anglin, J.R.: Dark–bright solitons in inhomogeneous Bose–Einstein condensates. Phys. Rev. Lett. **87**, 010401 (2001)
4. Dudley, J.M., Dias, F., Erkintalo, M., Genty, G.: Instabilities, breathers and rogue waves in optics. Nature Photon. **8**, 755 (2014)
5. Agrawal, G.P.: Applications of Nonlinear Fiber Optics. Academic Press, San Diego (2001)
6. Kibler, B., Fatome, J., Finot, C., Millot, G., Dias, F., Genty, G., Akhmediev, N., Dudley, J.M.: Observation of Kuznetsov-Ma soliton dynamics in optical fibre. Sci. Rep. **6**, 463 (2012)
7. Osborne, A.S.: Nonlinear Ocean Waves and the Inverse Scattering Transform. Academic Press, New York (2010)
8. Dudley, J.M., Taylor, J.M.: Supercontinuum Generation in Optical Fibers. Cambridge University Press, Cambridge (2010)
9. Kedziora, D.J., Ankiewicz, A., Chowdury, A., Akhmediev, N.: Integrable equations of the infinite nonlinear Schrödinger equation hierarchy with time variable coefficients. Chaos **25**, 103114 (2015)
10. Ankiewicz, A., Kedziora, D.J., Chowdury, A., Bandelow, U., Akhmediev, N.: Infinite hierarchy of nonlinear Schrödinger equations and their solutions. Phys. Rev. E **93**, 012206 (2016)
11. Serkin, V.N., Hasegawa, A.: Novel soliton solutions of the nonlinear Schrödinger equation model. Phys. Rev. Lett. **85**, 4502 (2000)

12. Akhmediev, N., et al.: Roadmap on optical rogue waves and extreme events. J. Opt. **18**, 063001 (2016)
13. Sulem, C., Sulem, P.-L.: The Nonlinear Schrödinger Equation. Springer, New York (1999)
14. Ankiewicz, A., Soto-Crespo, J.M., Akhmediev, N.: Rogue waves and rational solutions of the Hirota equation. Phys. Rev. E **81**, 046602 (2010)
15. Anderson, D., Lisak, M.: Nonlinear asymmetric self-phase modulation and self-steepening of pulses in long optical waveguides. Phys. Rev. A **27**, 1393 (1983)
16. Chowdury, A., Kedziora, D.J., Ankiewicz, A., Akhmediev, N.: Breather-to-soliton conversions described by the quintic equation of the nonlinear Schrödinger hierarchy. Phys. Rev. E **91**, 032928 (2015); Chowdury, A., Krolikowski, W.: Breather-to-soliton transformation rules in the hierarchy of nonlinear Schrödinger equations. Phys. Rev. E **95**, 062226 (2017)
17. Backus, S., Durfee III, C.G., Mourou, G., Kapteyn, H.C., Murnane, M.M.: 0.2-TW laser system at 1 kHz. Opt. Lett. **22**, 1256 (1997)
18. Xu, S.-L., Petrović, N., Belić, M.R.: Exact solutions of the (2 + 1)-dimensional quintic nonlinear Schrödinger equation with variable coefficients. Nonlinear Dyn. **80**, 583–589 (2015)
19. Mirzazadeh, M., Eslami, M., Zerrad, E., Mahmood, M.F., Biswas, A., Belić, M.: Optical solitons in nonlinear directional couplers by sine-cosine function method and Bernoulli's equation approach. Nonlinear Dyn. **81**, 1933–1349 (2015)
20. Biswas, A., Khalique, C.M.: Stationary solutions for nonlinear dispersive Schrödinger equation. Nonlinear Dyn. **63**, 623–626 (2011)
21. Chin, S.A., Ashour, O.A., Belić, M.R.: Anatomy of the Akhmediev breather: cascading instability, first formation time, and Fermi-Pasta-Ulam recurrence. Phys. Rev. E **92**, 063202 (2015)
22. Wu, X.-F., Hua, G.-S., Ma, Z.-Y.: Evolution of optical solitary waves in a generalized nonlinear Schrödinger equation with variable coefficients. Nonlinear Dyn. **70**, 2259–2267 (2012)
23. Trippenbach, M., Band, Y.B.: Effects of self-steepening and self-frequency shifting on short-pulse splitting in dispersive nonlinear media. Phys. Rev. A **57**, 4791 (1998)
24. Potasek, M.J., Tabor, M.: Exact solutions for an extended nonlinear Schrödinger equation. Phys. Lett. A **154**, 449 (1991)
25. Cavalcanti, S.B., Cressoni, J.C., da Cruz, H.R., Gouveia-Neto, A.S.: Modulation instability in the region of minimum group-velocity dispersion of single-mode optical fibers via an extended nonlinear Schrödinger equation. Phys. Rev. A **43**, 6162 (1991)
26. Wang, D.-S., Chen, F., Wen, X.-Y.: Darboux transformation of the general Hirota equation: multisoliton solutions, breather solutions and rogue wave solutions. Adv. Differ. Equ. **2016**, 67 (2016)
27. Guo, R., Hao, H.Q.: Breathers and multi-solitons solutions for the higher-order generalized nonlinear Schrödinger equation. Commun. Nonlinear Sci. Numer. Simul. **18**, 2426–2435 (2013)
28. Mani Rajan, M.S., Mahalingam, A.: Nonautonomous solitons in modified inhomogeneous Hirota equation: soliton control and soliton interaction. Nonlinear Dyn. **79**, 2469–2484 (2015)
29. Lan, Z., Gao, B.: Solitons, breather and bound waves for a generalized higher-order nonlinear Schrödinger equation in an optical fiber or a planar waveguide. Eur. Phys. J. Plus **132**, 512 (2017)
30. Chowdury, A., Kedziora, D.J., Ankiewicz, A., Akhmediev, N.: Breather solutions of the integrable nonlinear Schrödinger equation and their interactions. Phys. Rev. E **91**, 022919 (2015)
31. Chowdury, A., Kedziora, D.J., Ankiewicz, A., Akhmediev, N.: Soliton solutions of an integrable nonlinear Schrödinger equation with quintic terms. Phys. Rev. E **90**, 032922 (2014)
32. Yang, Y., Yan, Z., Malomed, B.A.: Rogue waves, rational solitons, and modulational instability in an integrable fifth-order nonlinear Schrödinger equation. Chaos **25**, 103112 (2015)
33. Chin, S.A., Ashour, O.A., Nikolić, S.N., Belić, M.R.: Maximal intensity higher-order Akhmediev breathers of the nonlinear Schrödinger equation and their systematic generation. Phys. Lett. A **380**, 3625–3629 (2016)
34. Schwalm, W.A.: Lectures on selected topics in mathematical physics: elliptic functions and elliptic integrals. Morgan & Claypool publication as part of IOP Concise Physics, vol. 68, San Rafael, CA, USA. (2015)
35. Nikolić, S.N., Aleksić, N.B., Ashour, O.A., Belić, M.R., Chin, S.A.: Systematic generation of higher-order solitons and breathers of the Hirota equation on different backgrounds. Nonlinear Dyn. **89**, 1637–1649 (2017)
36. Kedziora, D.J., Ankiewicz, A., Akhmediev, N.: Rogue waves and solitons on a cnoidal background. Eur. Phys. J. Spec. Top. **223**, 43–62 (2014)
37. Chin, S.A., Ashour, O.A., Nikolić, S.N., Belić, M.R.: Peak-height formula for higher-order breathers of the nonlinear Schrödinger equation on nonuniform backgrounds. Phys. Rev. E **95**, 012211 (2017)
38. Ashour O.A.: Maximal intensity higher-order breathers of the nonlinear Schrödinger equation on different backgrounds. In: Undergraduate Research Scholars Thesis, Texas A&M University, USA (2017)
39. Wang, L., Zhang, J.-H., Wang, Z.-Q., Liu, C., Li, M., Qi, F.-H., Guo, R.: Breather-to-soliton transitions, nonlinear wave interactions, and modulational instability in a higher-order generalized nonlinear Schrödinger equation. Phys. Rev. E **93**, 012214 (2016)
40. Zhang, J.-H., Wang, L., Liu, C.: Superregular breathers, characteristics of nonlinear stage of modulation instability induced by higher-order effects. Proc. R. Soc. A **473**, 20160681 (2017)